

**Excel**  
INDIA PUBLISHERS



**ICPCCS 12**

Proceedings of the International Conference on  
Perspectives of  
**Computer Confluence with Sciences 2012**

*10–12 December 2012*

*Organized by*



**Nowrosjee Wadia College**  
Pune

*in Association with*



University of Pune  
(BCUD)



**PERSISTENT**

Persistent Systems Ltd.



*Proceedings of the  
International Conference on  
Perspectives of Computer Confluence with Sciences  
(ICPCCS-12)*



10-12 December 2012

*Compiled by*  
Dr. Farhat Surve

*Organized by*  
Nowrosjee Wadia College, Pune, India  
(Affiliated to University of Pune)

*in Association with*



University of Pune  
(BCUD)



PERSISTENT  
Persistent Systems  
Ltd.

*Convener*  
Dr. K.V. Desa  
Head, Department of Physics

*Coordinator*  
Dr. S.C. Shirwaikar  
Head, Department of Computer Science

*Excel*  
INDIA PUBLISHERS

EXCEL INDIA PUBLISHERS  
New Delhi

# High-resolution Gulf Water Skin Temperature Estimation using TIR\ASTER

Pravin D. Kunte<sup>#1</sup>, Mani Murali, R.<sup>#2</sup>, Mahender, K<sup>\*3</sup>

<sup>#1,#2</sup>National Institute of Oceanography,  
Council of Scientific & Industrial Research,  
Dona Paula, Goa 403 004, India

<sup>1</sup>[kunte@nio.org](mailto:kunte@nio.org)

<sup>2</sup>[mmurali@nio.org](mailto:mmurali@nio.org)

<sup>3\*</sup>Department of Earth Science, Goa University, Goa, India

<sup>3</sup>[mkotha@yahoo.com](mailto:mkotha@yahoo.com)

**Abstract**----Advanced Space-borne Thermal Emission and Reflection Radiometer (ASTER) is the highest-resolution multi-spectral thermal infrared (TIR) sensor currently available on a polar-orbiting spacecraft which allows surface temperature estimation, at a spatial scale (90 m) that is suitable for detail studies. Water skin temperatures are estimated using five thermal infrared channels collected by the ASTER. In present article, an algorithm which converts the radiance values, that have been observed by the sensor, into the corresponding brightness temperature values, is documented. A possible relationship between estimated temperature and gulf morphologic features is investigated. Based on temperature variation, the Gulf of Khambat region is classified to separate geomorphic features. It is demonstrated that high resolution water skin temperature of small water bodies can be determined correctly, economically and less laboriously using space-based TIR/ASTER and that estimated temperature can be effectively used as an additional parameter to map certain morphometric features.

**Keywords:** ASTER, Gulf of Khambat, water skin temperature, TIR, algorithm.

## I. INTRODUCTION

The surface temperature of the land and ocean determines the energy of biogeochemical activity, the rate of heat flow and water transport between the surface and the atmosphere. On

land, soil and canopy, temperature is among the main determinants of the rate of growth of vegetation. Evapo-transpiration, snow and ice melt are highly sensitive to surface temperature fluctuation. For the oceans, the sea surface temperature influences the rate of growth of phytoplankton, the rate of absorption of carbon dioxide and other gases by sea water, and the rate of flow of heat to and from the atmosphere. In short, temperature products are key inputs to many of the algorithms that provide data for global temperature mapping and change observation. Space-based thermal sensors are attractive tools for collecting water surface (skin) temperatures. Unlike oceans, however, most inland lakes, Gulfs, and similar water bodies are too small to be measured by current spaced-based thermal sensors in high repeat orbits (e.g. MODIS, AVHRR, GOES, AATSR, GLI-2). Satellites with finer spatial resolution (e.g. ASTER, Landsat) have temporal resolutions enough to fill in the observation gaps, if utilized properly.

In past, NOAA-AVHRR data were used to derive Sea Surface Temperature (SST) to elucidate physical factors affecting the spatial distribution and abundance of harmful algal blooms [1]. The ERS satellites equipped with an along track scanning radiometer (ATSR) was used to measure the sea surface temperature for monitoring sea level and sea surface temperature trends [2]. Fronts in the Southern Indian Ocean were inferred from satellite sea surface temperature derived using AVHRR data [3]. Different coastal processes in Indonesian water

were investigated using SeaWiFS data in combination with temperature data from AVHRR [4]. Brightness temperature has been used to observe volcanic ash clouds [5], to measure thermal inertia [6], and detect ice leads in the Arctic [7] to name just a few examples.

#### A. Study area

The GoK is a funnel shaped indentation on the western shelf of India, lying between the Saurashtra peninsula and the mainland of Gujarat (Fig.1). The GoK is about 70 km wide and 130 km long bounded by latitudes  $21^{\circ}$  and  $22^{\circ} 20'$  N and longitudes  $72^{\circ}$  and  $73^{\circ}$  E. The coast of the GoK is marked by a number of estuaries, islands, mudflats, cliffs, salt marshes and mangrove swamps etc. The inner shelf of GoK is characterized by uneven seafloor topography. Depth ranges from a maximum of about 20 meters at the mouth to less than a meter at the head of the gulf.

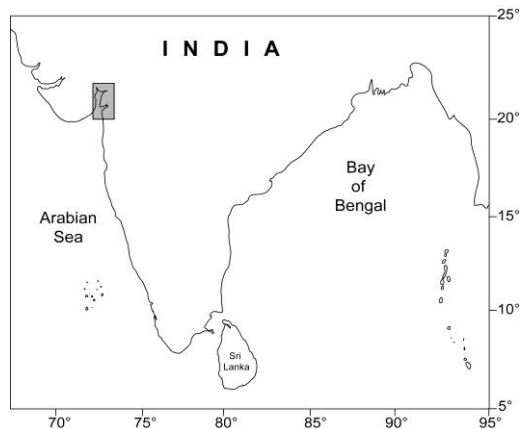


Fig. 1. Location map covering study area.

The Gulf comprises an area of high tides (up to 11 meters) and the largest amplitude on the west coast [8]. The coastal features are related to the behavior of tides and tidal currents. The amplitude increases as the tide moves into the GoK. The wind pattern in this area is predominantly seasonal with rare cyclonic disturbances. Predominant wind directions are west-southwesterly and north-northeasterly during the months June to September and December to March respectively. Higher wind speeds are likely to occur during June to September with winds up to 74 km/hr from the west and southwest [9].

In this article, an algorithm which converts the radiance values that have been observed by the sensor, into the corresponding brightness temperature values, is documented. A possible relationship between estimated temperature and gulf morphologic parameters is investigated with the hope that temperature can be used as an additional parameter to map gulf morphologic parameter.

## II. MATERIAL AND METHODS

Gulf surface temperatures are estimated using five thermal infrared (TIR) images collected by the ASTER (Advanced Space borne Thermal Emission and Reflection Radiometer), an imaging instrument flying on Terra, a satellite launched in December 1999 as part of NASA's Earth Observing System (EOS). ASTER is the highest-resolution multi-spectral TIR sensor currently available on a polar-orbiting spacecraft which allows surface temperature determination, at a spatial scale that allows detail studies.

ASTER is a multi-spectral scanner that produces images of high spatial resolution. Onboard Terra Satellite, the instrument has three bands in the visible and near-infrared (VNIR) spectral range (0.5-0.9  $\mu\text{m}$ ) with 15-m spatial resolution, six bands in the shortwave infrared (SWIR) spectral range (1.6-2.4  $\mu\text{m}$ ) with 30-m spatial resolution, and five bands in the thermal-infrared (TIR) spectral range (8-12  $\mu\text{m}$ ), with 90-m resolution. ASTER's estimated accuracy at 300 K is 1K and at 240K is 3 K. Radiometric precision (noise-equivalent temperature difference or NE $\Delta$ T) at 300 K is  $\leq 0.3$  K. A full description of the ASTER sensor and the Standard Products has been published [10]. For this study, three ASTER scenes from available standard products Level-3A01, captured on May 15<sup>th</sup> 2003, with a 60 $\times$ 60 km swath, covering GoK region were procured and used.

The radiance at the sensor is a function of the radiation emitted from the target and also the radiation emitted and absorbed by the intervening atmosphere, integrated over the response function of the sensor. The radiation emitted from the target at a given wavelength is a function of its temperature and emissivity. As atmospheric effects are overlooked while calculating brightness temperature at the sensor, the radiance at the sensor is the integral over the instrument response function of the emissivity

times the blackbody radiance. The temperature and the spectral emissivity are the two unknowns. By setting the emissivity to one, the temperature is calculated. In short the brightness temperature is considered as the temperature that a blackbody would be in order to produce the radiance acquired by the sensor.

The spectral radiance of a blackbody at temperature, T, and wavelength, λ, is given by the Planck's function.

$$L_{\lambda}^{BB} = \frac{c_1}{\lambda^5 \pi \left[ e^{\frac{c_2}{\lambda T}} - 1 \right]} \quad \text{----- 1}$$

Where:

$L_{BB}$  = blackbody radiance

(W/(m<sup>2</sup>\*steradian\*micron))

λ = wavelength (m)

T = temperature (°K)

C1 = first radiation constant = 2hc<sup>2</sup> = (1.19E-22 W\*m<sup>3</sup>/(steradian\*micron))

C2 = second radiation constant = hc/k = (0.0143877 m\*°K)

h: Planck's constant: 6.625\*10E(-34) [Joule\*sec]

k: Boltzmann's constant: 1.3804\*10E(-23) [Joule/K]

c: Velocity of light: 3.0E10 (+8) [m/sec]

Equation 1 is integrated over an instrument response function to calculate the radiance that corresponds to a brightness temperature for a particular instrument band.

$$L_s = \frac{\int \psi(\lambda) L^{BB}(T, \lambda) d\lambda}{\int \psi(\lambda) d\lambda} \quad \text{-----2}$$

Where:

$L_s$  = radiance observed by the sensor

ψ = instrument response

For solving for the temperature the easiest approximation is to replace the response function with a delta function at the sensor's central wavelength. Under this approximation, Equation 2 collapses into Equation 1, this can be inverted to

$$T_c = \frac{c_2}{\lambda_c \log \left( \frac{c_1}{\lambda_c^5 \pi L_s} + 1 \right)} \quad \text{----- 3}$$

Where:

$T_c$  = brightness temperature, from a central wavelength

$\lambda_c$  = the sensor's central wavelength.

The temperature in [K/ °C] is calculated from DN value using formula which is derived from Planck's formula. Temperature calculations are carried out in following steps :

Step 1 – Read DN value

Step 2 –  $L_s = (DN \text{ value}-1) * \text{conversion coefficient} * \pi(\text{Pi}) * 1000000$   
(watt\*m<sup>3</sup>/micron)

Step 3 - h v / k

Step 4 -  $1 + 2\pi hc^2 / \lambda^5 / \text{step 2}$

Step 5 – Log (step 4)

Step 6 – Step 3/ Step 5

Temperature in °C - step 6 – 273.15

Where,

$L_s = (DN \text{ value}-1) * \text{conversion coefficient}$   
(w/(m<sup>2</sup>\*steradian\*micron))

h: Planck's constant: 6.625\*10E(-34) [Joule\*sec]

k: Boltzmann's constant: 1.3804\*10E(-23) [Joule/K]

c: Velocity of light: 3.0E10 (+8) [m/sec]

T: Absolute Temperature[K]

λ: wave length of the thermal band

v: Frequency 1/sec

t : Temperature in degree centigrade

Conversion coefficients (Table 1) are used to convert DN values to radiance. Spectral radiance is expressed in unit of W/(m<sup>2</sup>\*sr\*µm). (For more details pl. refer: 5.2 radiometric parameters@[http://www.science.aster.ersdac.or.jp/en/documnts/users\\_guide/index2.html](http://www.science.aster.ersdac.or.jp/en/documnts/users_guide/index2.html))

**Table I**

Unit conversion coefficients

Thermal Bands	Maximum radiance (W/(m <sup>2</sup> *sr*µm))
10	6.882 x 10 <sup>-3</sup>
11	6.780 x 10 <sup>-3</sup>
12	6.590 x 10 <sup>-3</sup>
13	5.693 x 10 <sup>-3</sup>
14	5.225 x 10 <sup>-3</sup>

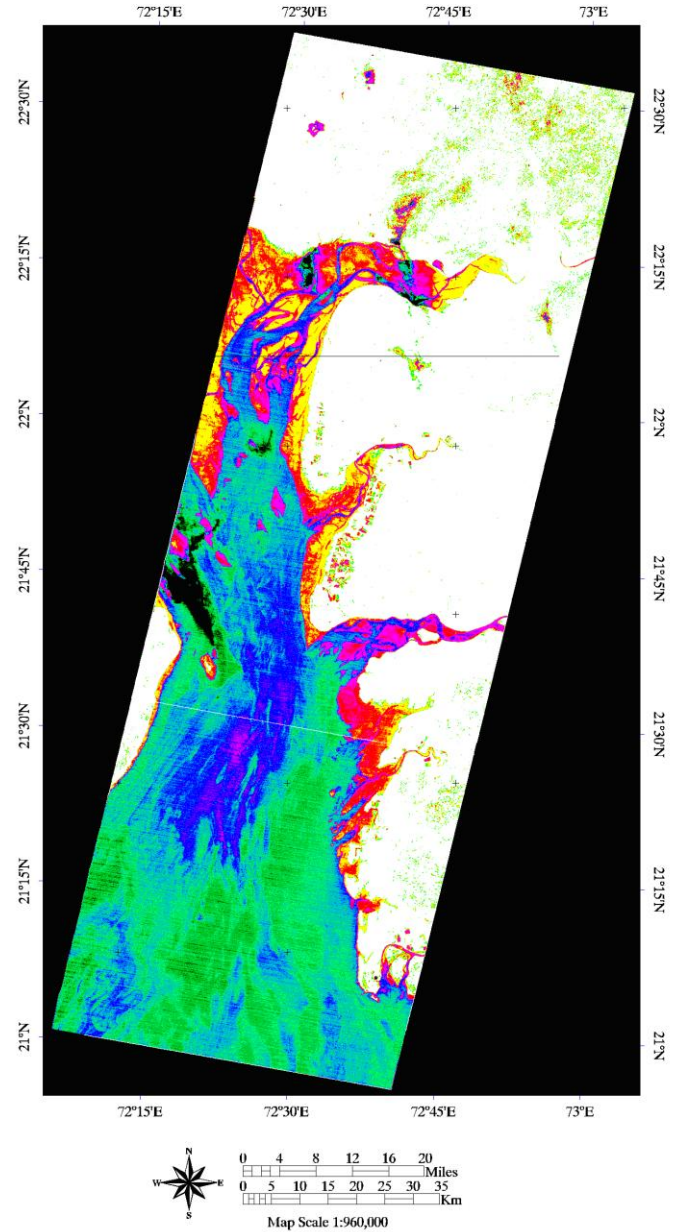
Adopting above methodology, five thermal bands of each three scenes were generated from respective TIR data files. The

temperature obtained from all 5 thermal bands is not same due to scattering and absorption. So to determine water skin temperature, following formula [11] is adopted and Multi-channel water skin temperature (MWST) images were generated.

$$MWST = 1.16 - 1.07 * T_{10} + 0.49 * T_{11} + 1.13 * T_{12} + 0.78 * T_{13} - 0.32 * T_{14} \text{ ----- } 4$$

The coefficients for surface temperature algorithm are derived from multiple regression analysis and are based on atmospheric transmission and radiance code for study area.

Using commercial GIS software package, three geo-referenced MWST maps were prepared and a mosaic was generated. Using image processing software, MWST image was density sliced and different colors were assigned to enhance the features. Seven geomorphic classes were identified and presented (Fig. 2). These MWST images were enlarged and visually analyzed, based on feature location, image characteristics and other associated features, various coastal geomorphic units were located and deciphered. Available navigation chart (NHC-208) and information obtained by visually interpreting the other ASTER channel images, were used for the confirmation of features.



Temperature range	Color	Geomorphic feature
21.6 to 28.0	Black	Cold and sediment free water
28.0 to 28.9	Green	Clear water
28.9 to 30.1	Light green	Less turbid water
30.1 to 31.5	Blue	Turbid water
32.0 to 35.0	Pink	Inter-tidal mudflats, Estuarine Island
35.5 to 36.0	Brick red	Sub-tidal mudflats and wet salt pans
36.0 to 40.0	Yellow	Dry palaeo-mudflats and dry salt pans

Fig. 2. Density sliced Gulf water skin temperature image.



### III. RESULT

Correlation coefficient between in-situ water skin temperature and water skin temperature estimated using TIR/ASTER data is shown in Figure 3. Differences within two data sets (Fig. 3) are probably due to data collection technique, resolution and date and time of data collection.

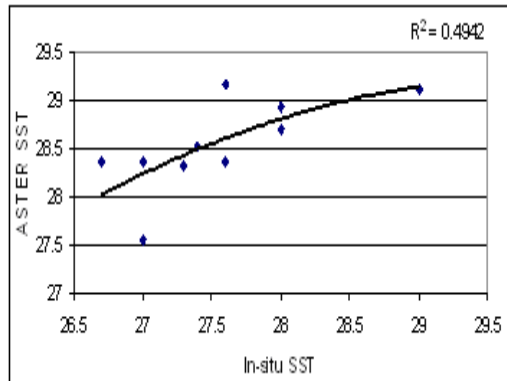


Fig. 3. Correlation coefficient between in-situ water skin temperatures and water skin temperature derived from ASTER

Estimated water skin temperature (MWST) data derived from ASTER was also compared with Level 3- Standard mapped SST image (Fig. 4) and weekly (9-16 May 2003) SST data with 4 km resolution derived from MODIS/TISIE (Data accessed from [http://oceancolor.gsfc.nasa.gov/cgi/level3.pl/A20031292003136.L3m\\_8DSST\\_4.png?DAY=12186&PER=8&TYP=masst&IMG=bigger](http://oceancolor.gsfc.nasa.gov/cgi/level3.pl/A20031292003136.L3m_8DSST_4.png?DAY=12186&PER=8&TYP=masst&IMG=bigger)).

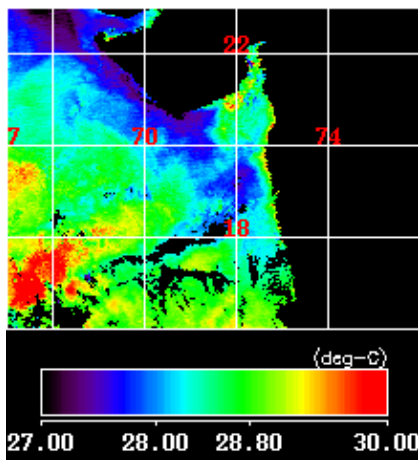


Fig. 4. Standard mapped SST image (Level 3) accessed from MODIS/TISIE

The comparison between water skin temperatures derived from MODIS/TISIE and ASTER/TES (Fig. 5) show  $R = 0.2321$  due to difference in spatial and temporal resolution.

From MWST image of three scenes, it is noted that temperature varies from  $20^{\circ}$  to  $40^{\circ}$  C within the Gulf region. Varied quantum of water content within various morphometric features causes disparity in surface temperature. Based on surface temperature variation, various geomorphic features like intertidal, subtidal and paleo-mudflats, river meander, estuarine islands, etc were differentiated and located. Presence of turbidity increases the temperature of water and so, clear and turbid waters were differentiated. Based on temperature variation, MWST image was classified and 7 geomorphic classes were identified. Gulf water was classified in four classes, clear water, less turbid water, turbid water and cold water entering from the Saurashtra coast. Inter-tidal mudflats and estuarine Islands could not be differentiated due to similar temperature range. However, islands are separable due to location and associated feature. Palaeo-mudflats and watery salt pans were differentiated based on typical salt pan pattern. Due to practical hindrance, no water skin temperature data was collected during satellite passes. However, in the absence of simultaneously collected data, surface temperature data collected one month ahead of ASTER data collection, during same summer season available with the data centre, was used as sea truth data.

### IV. DISCUSSION AND CONCLUSION

The correlation between water skin temperature estimated using above algorithm, in-situ water skin temperature and water skin temperature derived from MODIS data demonstrated that high resolution water skin temperature of small water bodies can be determined using space-based TIR/ASTER. A relationship between estimated temperature and gulf morphologic features show that based on temperature, the Gulf of Khambat region can be classified into various geomorphic features. It is thus concluded that high resolution water skin temperature of small water bodies can be determined economically and less laboriously using space-based TIR/ASTER and estimated

temperature can be used as an additional parameter to map certain morphological features.

Further, these derived surface temperatures (T) have several important applications viz., in global-change studies, in estimating radiation budgets and heat-balance studies, and as control for climate models. Brightness temperature can be used to observe volcanic ash clouds, to detect ice leads in the Arctic, and to identify anthropogenic and natural fires. Temperature data is useful in the monitoring and analysis of volcanic processes, day and night temperature data provided by ASTER is useful to estimate thermal inertia.

#### ACKNOWLEDGEMENT

We express our sincere gratitude to Dr. Satish Shetye, Director, National Institute of Oceanography for permitting us to publish this material. First author gratefully acknowledge Japan Society of Promotion of Science (JSPS), Japan for awarding a JSPS Postdoctoral Fellowship under which ASTER data was acquired. Sea truth data is obtained from Data Centre, NIO and MODIS SST data was accessed from <http://oceancolor.gsfc.nasa.gov/> web page. This is NIO contribution number

#### REFERENCES

- [1] Yu-Hwan Ahn, Palanisamy Shanmugam, Joo-Hyung Ryu, Jong-Chul Jeong, "Satellite detection of harmful algal bloom occurrences in Korean waters". *Harmful Algae* 5, 213–231, 2006.
- [2] O.B. Andersen, P. Knudsen, B. Beckley, "Monitoring sea level and sea surface temperature trends from ERS satellites", *Physics and Chemistry of the Earth*, 27, 1413-1417, 2002.
- [3] A.G. Kostianoy, a.I. Ginzburg, M. Frankignoulle, B. Delille, "Fronts in the Southern Indian Ocean as inferred from satellite sea surface temperature data", *Journal of Marine Systems*, 45(1-2), 55-73, 2004.
- [4] N. Hendiarti, H. Siegel, T. Ohde, " Investigation of different coastal processes in Indonesian waters using SeaWiFS data", *Deep-Sea Research-II*, 51, 85–97, 2004.
- [5] A.J. Prata, "Observations of volcanic ash clouds in the 10-12  $\mu\text{m}$  window using AVHRR/2 data".

*International Journal of Remote Sensing*, vol. 10(4, 5), 751-761, 1989.

- [6] P. Nasipur, T.J. Majumdar, D.S. Mitra, "Study of high-resolution thermal inertia over western India oil fields using ASTER data". *Acta Astronautica*, 58, 270-278, 2006.
- [7] R.S. Stone, "The Detectability of Arctic Leads using Thermal Imagery under varying Atmospheric Conditions". *Journal of Geophysical Research-Oceans*, 98(7), 2469-2482, 1993.
- [8] A.S. Unnikrishnan, S.R. Shetye, G.S. Michael, "Tidal propagation in the Gulf of Khambhat, Bombay High and surrounding areas", In: *Proceedings Indian Academy of Sciences (Earth and Planetary Science)*, 108(3), 155-177, 1999.
- [9] P.S. Srivastava, V.C. John, "Current regime in the Gulf of Kutch", *Indian Journal of Marine Sciences*, 6: 39-48, 1977
- [10] M. Abrams, S.J. Hook, B. Ramachandran, (2002). "ASTER user's handbook, version 2". <http://asterweb.jpl.nasa.gov/content/03data/04Documents/aster/userguidev2.pdf>.
- [11] T. Matsunaga, "Water surface temperature estimation using linear equation of brightness temperature observed by Advanced Spaceborne Thermal Emission and Reflection/Thermal Infrared Radiometer (ASTER/TIR)", *Journal of Remote Society of Japan*, 16(5), 2-13, 1996.



